

# Ultra-small phase estimation via weak measurement with postselection: A comparison of joint weak measurement and weak value amplification

Chen Fang\*,<sup>1</sup> Jing-Zheng Huang\*†,<sup>1</sup> Yang Yu,<sup>1</sup> Qin-Zheng Li,<sup>1</sup> and Gui-Hua Zeng‡<sup>1,2</sup>

<sup>1</sup>*State Key Laboratory of Advanced Optical Communication Systems and Networks,  
Shanghai Key Laboratory on Navigation and Location-based Service,  
and Center of Quantum Information Sensing and Processing,  
Shanghai Jiao Tong University, Shanghai 200240, China*

<sup>2</sup>*College of Information Science and Technology, Northwest University, Xian 710127, Shaanxi, China*

(Dated: April 19, 2019)

We derive a general theory for the joint weak measurement with arbitrary postselection and employ it in the time-delay measurement. Especially, we study two special cases, i.e., the balanced and unbalanced postselection regimes, and present an experiment to verify the theoretical results. The experimental results show that under similar conditions, the signal-to-noise ratio of using joint weak measurement scheme remains higher than 12 dB when the measured time-delay is smaller than the ultimate precision limit of the weak-value amplification scheme. Moreover, the joint weak measurement scheme is robust to the misalignment errors and the wavelength-dependency of optical components, which indicates its advantage of improving the measurement precision with convenient laboratory equipments.

PACS numbers:

## I. INTRODUCTION

Weak measurement with postselection, including weak-value amplification[1] and joint weak measurement[2], provide a new technique for precision measurements and attract increasing attention in the recent years[3–5]. The main idea behind is that postselection can improve estimation precision in the presence of technical restrictions[6–8]. In particular, weak-value amplification gives advantages in suppressing certain kinds of technical noises and realistic limitations, such as detector saturation, correlated noises and angular beam jitter[8], thus make it easier to reach the quantum standard limit with common experimental equipments[9]. Moreover, Brunner and Simon[10] pointed out that in phase-shift or time-delay measurements, the weak-value amplification scheme can provide 3-orders of magnitude improvement on measurement precision over the standard interferometry when similar alignment errors are taken into account[11, 12].

However, two disadvantages exist in the weak-value amplification scheme. First, systematic errors and alignment errors set limits on the measurement precision[10, 11]. Second, in the weak-value amplification scheme, only a small fraction of events survive after the postselection process and a large amount of unselected events are unused, which seriously reduce its efficiency[13]. To improve this technique, it is natural to consider the benefit of picking up the unselected data[14, 15]. In Ref.[2], Strübi and Bruder proved that by carrying out joint weak measurement, namely a full joint measurement on both selected and unselected events, one can not only increase the efficiency but also remove systematic errors and alignment errors as the limiting factors. In theory, joint

weak measurement has no ultimate precision limit[2, 7].

In this work, we demonstrate the idea of joint weak measurement in a time-delay measurement experiment and show advantages of this technique over the weak-value amplification scheme. In Sec.II, we generate a formalism for weak measurement with arbitrary postselection, and derive an analytic formula for estimating the time-delay. Different from the original proposal in [2], there is no restriction to the post-selected state, thus the weak-value amplification scheme[10] and the joint weak measurement scheme[2] can be considered as two special scenarios in our theory. In Sec.III, we testify our theory by demonstrating a time-delay experiment. When the measuring time-delay is smaller than the measurable limit of the weak-value amplification scheme, an over 12 dB signal-to-noise ratio can still be achieved by using joint weak measurement. Finally, we conclude the results and outlooks related to our work in Sec.IV.

## II. THEORY

### A. General Theory

Consider a weak measurement scenario involving a two-level ancillary system in a quantum state  $|\varphi\rangle$  and a meter with its wave function of  $\phi(p)$  (where  $p$  is the degree of freedom readout from the related pointer). The interaction between the system and the meter is described by an unitary operator  $\hat{U}_{int} = e^{-ig\hat{A}\hat{p}}$ , where  $\hat{A}$  acts on the system with eigenvalues of 1 and  $-1$ ,  $\hat{p}$  is the momentum operator acting on the meter and  $g$  is the coupling strength. The effect of this operator is a rotation of the system state on a Bloch sphere, therefore can be expressed as

$$\hat{U}_{int} = e^{-ig\hat{A}\hat{p}} = \cos(g\hat{p})\hat{\mathbb{I}} - i \sin(g\hat{p})\hat{A} \quad (1)$$

After the interaction, the initial state  $|\Psi\rangle = |\varphi_i\rangle \otimes |\phi\rangle$

\*These authors contributed equally to this work.

†jzhuang1983@sjtu.edu.cn

‡ghzeng@sjtu.edu.cn

evolves to

$$\begin{aligned} |\Psi'\rangle &= \hat{U}_{int}|\varphi_i\rangle|\phi\rangle \\ &= [\cos(gp)|\varphi_i\rangle - i \sin(gp)\hat{A}|\varphi_i\rangle]|\phi\rangle \end{aligned} \quad (2)$$

The ancillary system is then postselected by two orthogonal states,  $|\varphi_{f1}\rangle$  and  $|\varphi_{f2}\rangle$ , and makes the pointer state converts to

$$\begin{aligned} |\phi'_j\rangle &= \langle\varphi_{fj}|\Psi'\rangle \\ &= [\cos(gp)\langle\varphi_{fj}|\varphi_i\rangle - i \sin(gp)\langle\varphi_{fj}|\hat{A}|\varphi_i\rangle]|\phi\rangle \\ &= \langle\varphi_{fj}|\varphi_i\rangle[\cos(gp) - i \sin(gp)\frac{\langle\varphi_{fj}|\hat{A}|\varphi_i\rangle}{\langle\varphi_{fj}|\varphi_i\rangle}]|\phi\rangle, \end{aligned} \quad (3)$$

where  $j = 1, 2$ . Consequently, the probability distribution of  $p$  associated with the pointer becomes

$$\begin{aligned} P'_j(p) &\equiv |\langle p|\phi'_j\rangle|^2 \\ &= |\langle\varphi_{fj}|\varphi_i\rangle|^2|\cos(gp) - i \sin(gp)A_{wj}|^2|\langle p|\phi\rangle|^2 \\ &= |\langle\varphi_{fj}|\varphi_i\rangle|^2|\langle p|\phi\rangle|^2 \\ &\quad \times \{[\cos(gp) + \sin(gp)ImA_{wj}]^2 + \sin^2(gp)(ReA_{wj})^2\} \\ &= |\langle\varphi_{fj}|\varphi_i\rangle|^2|\langle p|\phi\rangle|^2 \\ &\quad \times [\cos^2(gp) + \sin^2(gp)|A_{wj}|^2 + \sin 2(gp)ImA_{wj}] \\ &\equiv |\langle\varphi_{fj}|\varphi_i\rangle|^2P_0(p)\zeta_j(p, g), \end{aligned} \quad (4)$$

where  $A_{wj} \equiv \frac{\langle\varphi_{fj}|\hat{A}|\varphi_i\rangle}{\langle\varphi_{fj}|\varphi_i\rangle}$  is the well known weak value[16],  $P_0(p) \equiv |\langle p|\phi\rangle|^2$  is the initial probability distribution about  $p$  of the pointer, and  $\zeta_j(p, g) \equiv \cos^2(gp) + \sin^2(gp)|A_{wj}|^2 + \sin 2(gp)ImA_{wj}$  is the part changing the shape of the initial distribution.

Based on Eq.(4), one can estimate  $g$  making use of the maximum-likelihood estimation method[2, 7, 23]. Our derivation below is applicable to arbitrary postselection and is not restricted to the phase-shift measurement.

We begin with constructing the log-likelihood estimator

$$\begin{aligned} L(g) &= \sum_j \int dp Q_j(p) \log P(f_j, p) \\ &= \sum_j \int dp Q_j(p) [\log P_0(f_j, p) + \log \zeta(p, g)], \end{aligned} \quad (5)$$

where  $Q_j(p)(j = 1, 2)$  is the realistic probability distribution of  $p$  revealed from experimental data, with  $\int dp [Q_1(p) + Q_2(p)] = 1$ . To maximize the log-likelihood estimator, one should make  $\frac{\partial L}{\partial g} = 0$  and get:

$$\begin{aligned} \frac{\partial L}{\partial g} &= \sum_j \int dp Q_j(p) \frac{\partial \log \zeta}{\partial g} \\ &= \sum_j \int dp Q_j(p) \frac{p[\sin 2(gp)(|A_{wj}|^2 - 1) + 2 \cos 2(gp)ImA_{wj}]}{\cos^2(gp) + \sin^2(gp)|A_{wj}|^2 + \sin 2(gp)ImA_{wj}} \\ &= 0. \end{aligned} \quad (6)$$

The weak measurement requires  $gp \ll 1$  and  $|A_w|gp \ll 1$ [17]. Using the approximation  $\sin gp \approx gp$ , the above equation is simplified as

$$\sum_j \int dp Q_j(p) \frac{-2 \text{Im} A_{wj} p^3 g^2 + (|A_{wj}|^2 - 1) p^2 g + \text{Im} A_{wj} p}{(|A_{wj}|^2 - 1) p^2 g^2 + 2 \text{Im} A_{wj} g p + 1} = 0, \quad (7)$$

Solving the above equation provides a maximum-likelihood estimate of  $g$ . We note that there could be more than one solutions. One should substitute them back to the equation

and check which one can maximize the estimator. Interestingly, our derivations applying maximum likelihood estimation method on weak measurement do not require prior knowledge about the initial pointer wave function  $\varphi(p)$ .

Generally, the analytical solutions of Eq.(7) is difficult to obtained. Fortunately, under the condition of  $|A_w|gp \ll 1$ , Eq.(7) can be approximately simplified to a quartic equation,

$$Ag^4 + Bg^3 + Cg^2 + Dg + E = 0, \quad (8)$$

where

$$\begin{aligned} A &= \sum_j \int dp Q_j(p) p^5 [2(|A_{wj}|^2 - 1) \text{Im} A_{wj}], \\ B &= \sum_j \int dp Q_j(p) p^4 [4(\text{Im} A_{wj})^2 - (|A_{wj}|^2 - 1)^2], \\ C &= \sum_j \int dp Q_j(p) p^3 [\text{Im} A_{wj} (1 - 3|A_{wj}|^2)], \\ D &= \sum_j \int dp Q_j(p) p^2 [(|A_{wj}|^2 - 1) - 2 \text{Im} A_{wj}], \text{ and} \\ E &= \sum_j \int dp Q_j(p) p \text{Im} A_{wj}. \end{aligned}$$

As  $p$  is extremely small, one may obtain the first-order approximate solution

$$g_{est}^{(1)} = -\frac{E}{D} = \frac{\sum \text{Im} A_{wj} \langle p \rangle_j}{\sum [2(\text{Im} A_{wj})^2 - |A_{wj}|^2 + 1] \langle p^2 \rangle_j}, \quad (9)$$

where  $\langle p \rangle_j = \int dp Q_j(p) p$  and  $\langle p^2 \rangle_j = \int dp Q_j(p) p^2$ . It provides an appropriate estimation of  $g$  with very high precision.

## B. Time-delay measurement

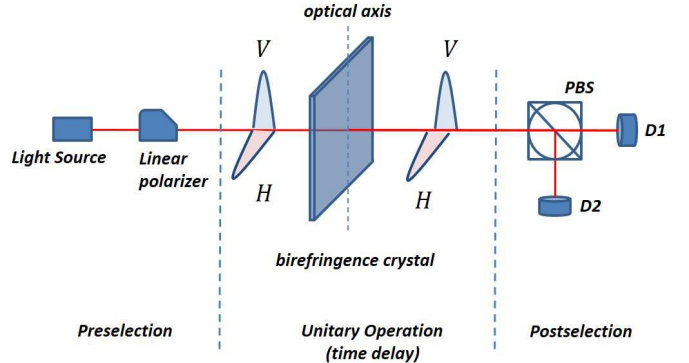


FIG. 1: (Color online). Time-delay measurement. Photons emitted from a light source is modulated to be a linear superposition state of two orthogonal polarizations,  $H$  and  $V$ , by a linear polarizer. After passing through a thin birefringent crystal, a small time delay is involved between the two polarizations. The postselection is performed by a circular polarization beam splitter(PBS) and the output lights are collected by two spectrometers (D1 and D2).

As a specific application in our theory, we consider a time-delay measurement described in Fig.1. In this scheme, a time delay of  $\tau$  is involved by a birefringent crystal between two orthogonal polarizations, which are denoted as horizontal ( $H$ ) and vertical ( $V$ ). The corresponding unitary operator is given by

$$\hat{U}_{int}(\tau) = e^{-i\tau\hat{\sigma}_Z\omega}, \quad (10)$$

where  $\hat{\sigma}_Z = |H\rangle\langle H| - |V\rangle\langle V|$  is the Z operator acting on the polarization and  $\omega$  represents the frequencies of the propagate photons.

Given an initial state of  $|\varphi_i\rangle = \frac{|H\rangle+|V\rangle}{\sqrt{2}}$  and post-selected states of  $|\varphi_{f1}\rangle = \frac{|H\rangle+e^{i\phi}|V\rangle}{\sqrt{2}}$  and  $|\varphi_{f2}\rangle = \frac{|H\rangle-e^{i\phi}|V\rangle}{\sqrt{2}}$ , we get the weak values

$$\begin{aligned} A_{w1} &= \frac{\langle\varphi_{f1}|\hat{A}|\varphi_i\rangle}{\langle\varphi_{f1}|\varphi_i\rangle} = \frac{1-e^{-i\phi}}{1+e^{-i\phi}} = i \tan(\frac{\phi}{2}) \\ A_{w2} &= \frac{\langle\varphi_{f2}|\hat{A}|\varphi_i\rangle}{\langle\varphi_{f2}|\varphi_i\rangle} = \frac{1+e^{-i\phi}}{1-e^{-i\phi}} = -i \cot(\frac{\phi}{2}). \end{aligned} \quad (11)$$

The successful probabilities are given by

$$\begin{aligned} P_{f1} &= |\langle\varphi_{f1}|\varphi_i\rangle|^2 \int d\omega P_0(\omega) \zeta_1(\omega, \tau) \\ &= \cos^2 \frac{\phi}{2} [1 + (\tan^2 \frac{\phi}{2} - 1) \omega_0^2 \tau^2 + 2 \tan \frac{\phi}{2} \omega_0 \tau]; \\ P_{f2} &= |\langle\varphi_{f2}|\varphi_i\rangle|^2 \int d\omega P_0(\omega) \zeta_2(\omega, \tau) \\ &= \sin^2 \frac{\phi}{2} [1 + (\cot^2 \frac{\phi}{2} - 1) \omega_0^2 \tau^2 - 2 \cot \frac{\phi}{2} \omega_0 \tau], \end{aligned} \quad (12)$$

where  $\omega_0 \equiv \int P_0(\omega) \omega d\omega$  represents the initial average frequency of light before the interaction. In practice,  $P_{f1}$  and  $P_{f2}$  can be estimated from experimental data by  $\int Q_1(\omega) d\omega$  and  $\int Q_2(\omega) d\omega$ , respectively.

Inserting Eq.(11) into Eq.(9) gives

$$\begin{aligned} \tau_{est}^{(1)} &= \frac{\tan \frac{\phi}{2} (\omega_1 - \cot \frac{\phi}{2} \omega_2)}{(\tan^2 \frac{\phi}{2} + 1) (\omega_1^2 + (\cot^2 \frac{\phi}{2} + 1) \omega_2^2)} \\ &= \frac{\sin^2 \frac{\phi}{2} (\omega_1 - \cos \frac{\phi}{2} \omega_2)}{\sin \frac{\phi}{2} \cos \frac{\phi}{2} (\omega_1^2 / \cos^2 \frac{\phi}{2} + \omega_2^2 / \sin^2 \frac{\phi}{2})} \\ &= \frac{\sin^2 \frac{\phi}{2} (\omega_1 - \cos^2 \frac{\phi}{2} \omega_2)}{\tan \frac{\phi}{2} (\omega_1^2 + \cot \frac{\phi}{2} \omega_2^2)}. \end{aligned} \quad (13)$$

In this derivation  $\tau$  and  $\omega$  are replaced by  $g$  and  $p$ , respectively. We note that estimating  $\tau$  from Eq.(13) requires prior knowledge on  $\phi$ .

In follows, we discuss two special cases, i.e., the *nearly balanced postselection* regime ( $P_{f1} \approx P_{f2}$ ) corresponding to the proposal in Ref.[2], and the *extremely unbalanced postselection* regime ( $P_{f1} \gg P_{f2}$ ) corresponding to the weak-value amplification scheme setting.

(1) Balanced postselection. In this regime, the light intensities detected by two spectrometers are nearly equal, which requires  $\phi \approx \frac{\pi}{2}$ . The successful postselection probabilities of two output ports are

$$\begin{aligned} P_{f1} &\approx \cos^2 \frac{\phi}{2} (1 + 2 \tan \frac{\phi}{2} \omega_0 \tau). \\ P_{f2} &\approx \sin^2 \frac{\phi}{2} (1 - 2 \cot \frac{\phi}{2} \omega_0 \tau). \end{aligned} \quad (14)$$

Then Eq.(13) is simplified as

$$\begin{aligned} \tau_{jw} &\approx \frac{P_{f1}(\omega_2) - P_{f2}(\omega_1)}{(\langle\omega^2\rangle_1 + \langle\omega^2\rangle_2) - \omega_0(\langle\omega\rangle_1 + \langle\omega\rangle_2)} \\ &= \frac{P_{f1}(\omega_2) - P_{f2}(\omega_1)}{\Delta\omega^2}. \end{aligned} \quad (15)$$

With this formula in hand, we can estimate  $\tau$  without being precisely aware of  $\phi$ . We note that this result is conflict with the formula given in [2], which is:  $\tau = \frac{1}{4}(\frac{\langle\omega\rangle_2 - \langle\omega\rangle_1}{\Delta\omega^2} - \frac{P_{f2} - P_{f1}}{\Delta\omega})$ . In Sec.III we will further verify the correctness of our formula by experiment.

(2) Unbalanced postselection. In this regime, most of the light output from port 1, which requires  $\phi \approx 0$ . The successful

postselection probabilities of the two output ports are

$$\begin{aligned} P_{f1} &\approx (1 - \frac{\phi^2}{4})[1 + \phi\omega_0\tau]. \\ P_{f2} &\approx \frac{\phi^2}{4}[1 - \frac{4}{\phi^2}\omega_0\tau]. \end{aligned} \quad (16)$$

In this case, Eq.(13) gives

$$\tau_{wva} = \frac{\frac{\phi}{2}(\overline{\langle\omega\rangle}_1 - \overline{\langle\omega\rangle}_2)}{\overline{\langle\omega^2\rangle}_1 + \overline{\langle\omega^2\rangle}_2 - 2\omega_0\overline{\langle\omega\rangle}_2}, \quad (17)$$

where  $\overline{\langle\omega\rangle}_j \equiv \frac{\int Q_j(\omega) \omega d\omega}{\int Q_j(\omega) d\omega} = \langle\omega\rangle_j / P_{fj}$  and  $\overline{\langle\omega^2\rangle}_j \equiv \frac{\int Q_j(\omega) \omega^2 d\omega}{\int Q_j(\omega) d\omega} = \langle\omega^2\rangle_j / P_{fj}$ .

In Eq.(17), we have  $\overline{\langle\omega\rangle}_1 - \overline{\langle\omega\rangle}_2 \approx \omega_0 - \overline{\langle\omega\rangle}_2 \equiv \delta\omega$  and  $\overline{\langle\omega^2\rangle}_1 + \overline{\langle\omega^2\rangle}_2 - 2\omega_0\overline{\langle\omega\rangle}_2 \approx 2\langle\Delta\omega^2\rangle$ . Consider that  $A_{w2} = -i \cot(\frac{\phi}{2}) \approx -i\frac{2}{\phi}$ , we recover the WVA expression[11]:  $\overline{\langle\omega\rangle}_1 - \overline{\langle\omega\rangle}_2 \approx \frac{4}{\phi}\langle\Delta\omega^2\rangle\tau_{est} \rightarrow \delta\omega \approx 2\tau_{est} Im A_{w2} \langle\Delta\omega^2\rangle$ , thus include WVA as a special case of our theory.

### III. EXPERIMENT

#### A. Experimental Setup

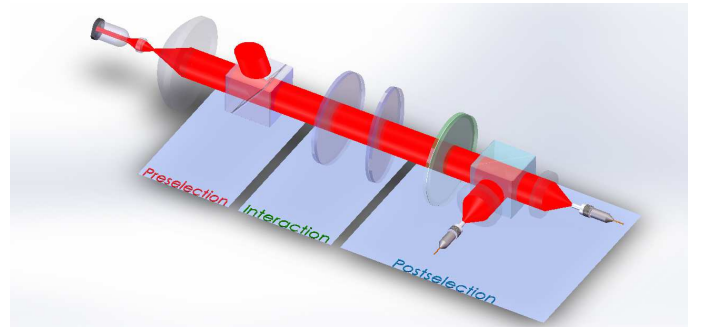


FIG. 2: (Color online). Experimental setup of the time delay measurement. Photons emitted from a light emitted diode (LED) with center wavelength of 780nm and line width of  $\Delta\lambda = 17.6nm$  are collimated by an aspheric lens and a convex plane lens then enter the Glan-Taylor prism, which preselects the polarization state  $|\varphi_i\rangle = \frac{1}{\sqrt{2}}(|H\rangle + |V\rangle)$ . After that, the light passes through two compound binary zero-order half-wave plates (HWP) with their optical axes (OAs) perpendicular to each other and at  $45^\circ$  to the polarization of the prism. The second HWP is pivoted by a small angle  $\theta$  around its OA. Postselection is realized by a combination of a compound binary zero-order quarter-wave plate (QWP) and a polarization beam splitter (PBS). The photons are split into two orthogonal polarized beams and focused into optical fibers by lenses, then sent to two spectrometers with sampling resolution of 0.1 nm and range of 690-900 nm.

We design an experiment to demonstrate the time delay measurement and verify our theory presented in Sec.II B. The experimental setup is described in fig.2. In Fig.1, a thin birefringent crystal is used to induce the time delay. However in practice, it is very difficult to produce and manipulate this

kind of plate. Follow the idea in Ref.[12], we use a double-plate system with placing their optical axes(OAs) perpendicularly to each other to equivalently realize this effect. Restricted by the laboratory condition, we use the binary compound zero-order half-wave plates (HWPs) in our experiment. These plates are built by combining two multi-order wave plates and aligning the fast axis of one plate with the slow axis of the other to obtain the zero-order phase delay. In contrast to the true zero-order plates used in [12], they are insensitive to the temperature changes. We place both plates perpendicularly to the light velocity to cancel their phase delay. The delay is realized by pivoting the second plate around its OA by a tiny angle  $\theta$ . This pivot increases the optical path of the second HWP, which makes the double-HWPs system equivalent to a very thin plate of the same material with the OA orienting as the tilted one. The relationship between the time delay  $\tau$  and the tilt angle  $\theta$  is

$$\tau = \frac{(n_e - n_o)h\theta^2}{2c\lambda n^2}, \quad (18)$$

where  $n_e$ ,  $n_o$  and  $n$  are the refractive indices of quartz for extraordinary light, ordinary light and average, respectively,  $h$  is the thickness of the plate,  $c$  is the light speed and  $\lambda$  is the wavelength of the light. For detailed derivations, see Appendix. A and Ref.[26].

Finally, in order to finish the postselection, the photons sequentially enter a quarter-wave plate (QWP) and a polarization beam splitter (PBS). Originally, the OA of the QWP is perpendicular to the axis of the Glan-Taylor prism and the PBS splits the photons to polarization states  $|H\rangle$  and  $|V\rangle$ . And then, the PBS is rotated by an angle of  $\gamma = \pi/4 - \frac{\phi}{2}$  according to the GT prism's OA orientation to postselect final states of  $|\varphi_{f1}\rangle = \cos\gamma|H\rangle + \sin\gamma|V\rangle$  and  $|\varphi_{f2}\rangle = \sin\gamma|H\rangle - \cos\gamma|V\rangle$ .

In our setting, when  $\phi \approx \frac{\pi}{2}$ , the light intensities go out from the two output ports are nearly the same, which corresponds to the proposal of [2], and we call it here the "balanced" postselection regime. In contrast when  $\phi \approx 0$ , almost all of the light go out from one output port, which is similar to the weak-value amplification scheme, and we call it here the "unbalanced" postselection regime. In the following, we will present the experimental results of these two regimes to verify the theory derived in Sec.II.

## B. Balanced and unbalanced postselection regimes

*Balanced postselection regime* – In this regime, we set  $\phi \approx (\frac{\pi}{2} + 0.071) \text{ rad}$  (by rotating the PBS with an angle of  $-0.071 \text{ rad}$ ), and the postselection probabilities for each output port can be calculated by Eq.(14). In Fig.3, according to the tilted angle we made, different estimations about the time-delay are shown, where the theoretical predictions drawn by blue line are calculated by Eq.(18). Among these estimations, blue triangles are the complete solutions to Eq.(7), when red circles and black crosses are the approximate solutions given by Eq.(13) and Eq.(15) respectively. Compared to Eq.(13), Eq.(15) does not require the prior knowledge about  $\phi$ , this parameter is estimated by the light intensity difference of the

two output ports. However Eq.(15) provides an estimation with less accuracy, because the environment effects, such as the fluctuation of the temperature, make the output intensity of the LED unstable .

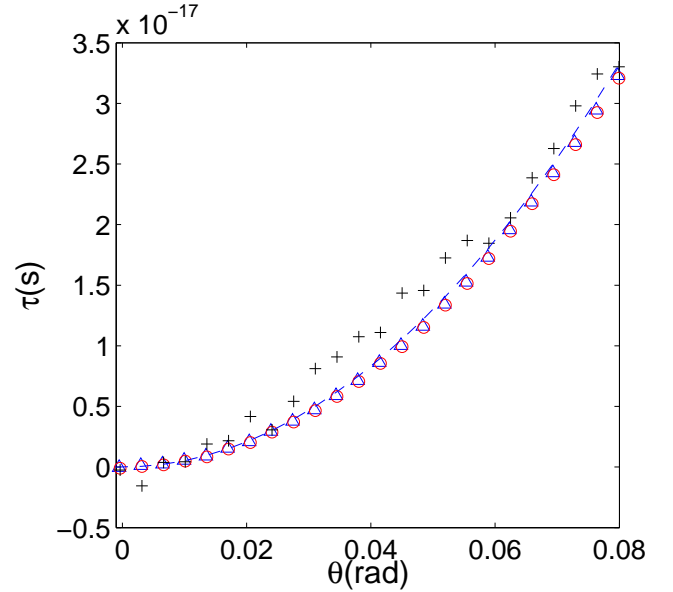


FIG. 3: (Color online.) Relation of  $\theta$  and  $\tau$  in the *balanced* postselection regime. Blue line presents the theoretical prediction from Eq.(18), blue triangles, red circles and black crosses are estimations from experimental data, calculated by Eq.(7), Eq.(13) and Eq.(15) respectively.

*Unbalanced postselection regime* – In this regime, we set  $\phi \approx 0.03$  (by rotating the PBS for  $\pi/4 - 0.03 \text{ rad}$ ), and the postselection probabilities for each output port, which can be calculated by Eq.(16), are extremely unbalanced. In Fig.4, according to the tilted angle we made different estimations about the time-delay are shown, where the theoretical predictions drawn by blue line are calculated by Eq.(18). Among these estimations, blue triangles are the complete solutions to Eq.(7), when red circles are the approximate solutions given by Eq.(13).

We can find that the red circles fit well with the theory as the red patterns when  $\tau$  is less than  $0.5 \times 10^{-17}$  but the deviation creases along with the growing  $\tau$ , because the effect of wavelength dependency of the quarter-wave plate was not taken into account in Eq.(17) (see Appendix. B for details).

## C. Discussions

Utilizing the imaginary part of weak value provides a large amplification factor for parameter estimation. For introducing imaginary weak value it requires a circular component in the polarization by inserting a quarter-wave plate. However, as is pointed out in [12], the quarter-wave plate involves large uncertainty to the polarization that is difficult to compensate, because of the wide spectrum of the light we used.

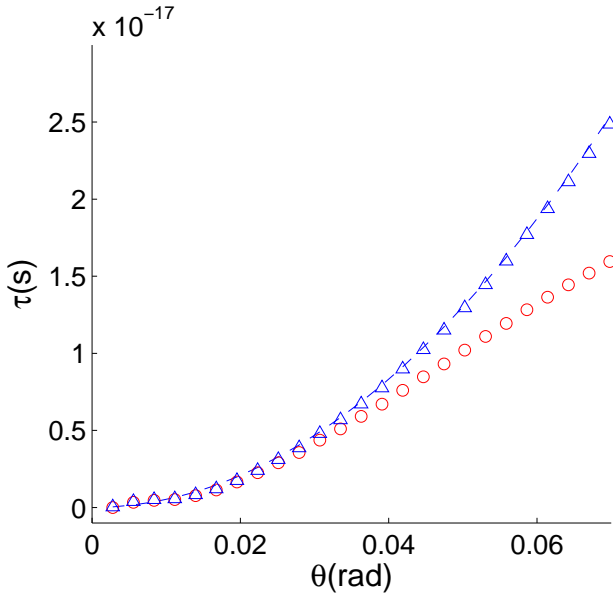


FIG. 4: (Color online.) Relation of  $\theta$  and  $\tau$  in the *unbalanced* post-selection regime. Blue line presents the theoretical prediction from Eq.(18), blue triangles and red circles are the estimation of  $\tau$  derived from experimental data, calculated by Eq.(7) and Eq.(13) respectively.

There are two possible ways to solve this problem: get rid of the quarter-wave plate with the price of much smaller weak value, or apply joint weak measurement method to surpass the wavelength-dependence effect.

Consider both of the proposals in the unbalanced postselection regime. Removing the quarter-wave plate in our experimental setting (see fig.2) reverts a similar set-up as in [12]. Alternatively, we can collect the data from both output sides and apply Eq.(9) for estimation. When  $\tau$  is small enough so that  $|A_w|\omega_0\tau \ll 1$  is satisfied, the estimation fit quite well to the theoretical prediction (see fig.4).

In [12], the uncertainty of measuring  $\alpha$  (equals  $\omega_0\tau$  in our paper) depends on the spectrometer resolution  $\Delta(\delta\lambda)$  and the postselection parameter  $\beta$  (equals  $2\gamma$  in our paper). The uncertainty of  $\alpha$ , which is denoted as  $\Delta\alpha$ , can be derived as[12]:

$$\Delta\alpha = \frac{\lambda_0}{4\Delta\lambda^2} \cdot \frac{(\alpha^2 + \beta^2)^2}{\alpha\beta^2} \cdot \Delta(\delta\lambda). \quad (19)$$

According to this formula, the optimal precision can be achieved when  $\beta \simeq \alpha$ , but it is very impractical because the value of  $\alpha$  is unknown before it is measured. Alternatively, the authors pointed out that for measuring small  $\alpha$  one can set  $\beta = 0$  and obtain  $\Delta\alpha \simeq 0.1\alpha$  when  $\Delta(\delta\lambda) = 0.1nm$ . However, an important factor, the misalignment of  $\beta$ , had not been considered. In fact, it sets a limitation on the minimum detectable phase when using weak value amplification[10]. Assume that the actual value of  $\beta$  is  $\epsilon$  when we set it to be 0, and consider  $\alpha_{min} = \Delta\alpha$  as the minimum detectable value of the measured phase, we can derive from Eq.(19) that

$$\alpha_{min} = \sqrt{\frac{\sqrt{1-4C}-2C+1}{2C}}\epsilon, \quad (20)$$

where we define  $C \equiv \frac{\lambda_0}{4\Delta\lambda^2}\Delta(\delta\lambda)$  for simplicity. By setting  $\Delta(\delta\lambda) = 0.1nm$ , which is assumed in [12] and practically applied in our experiment, we get  $\alpha_{min} \simeq 3.7\epsilon$ .

On the other hand, by using the joint weak measurement scheme proposed in [2] and demonstrated in Sec.III B, the uncertainty of measured phase is insensitive to the alignment error. In our experiment, we set  $\phi = 0.03$ . The exact value of  $\phi$  can be estimated by maximizing Eq.(7), but it is not necessary to do so for achieving high precision. In Fig.5 we calculate the signal-to-noise ratio(SNR) when estimating  $\tau$  by Eq.(9) and setting  $\phi = 0.03, 0.05$  and  $0.08$  rad respectively. The SNR drops slightly even when our prediction about  $\phi$  has a deviation of 0.05 rad, and remains higher than 10 dB for  $\alpha > 0.002$ . It shows that the estimation results are insensitive to  $\phi$  in balanced postselection regime. In contrast, for weak value amplification in unbalanced postselection regime, for a typical deviation of  $\epsilon = 0.0027$ [12], SNR drops down to 0 dB when  $\alpha = 0.01$ , much worse than applying the joint weak measurement method.

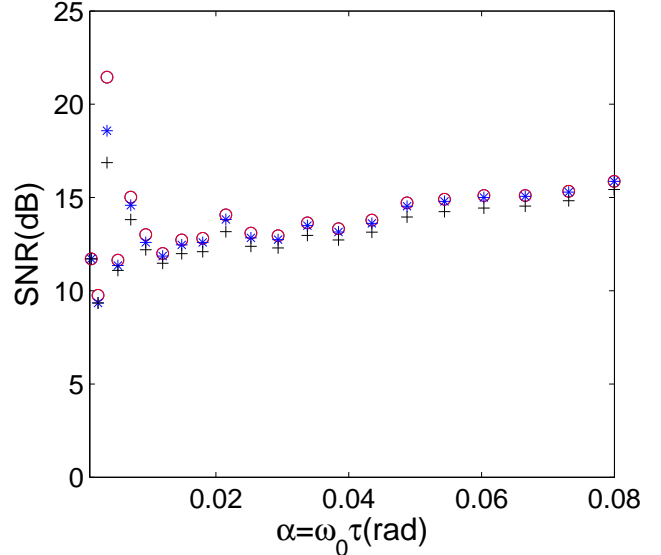


FIG. 5: Signal-to-noise ratio in the time-delay measurement experiment with balanced postselection. Red circles:  $\phi = 0.03$ ; Blue stars:  $\phi = 0.05$ ; Black crosses:  $\phi = 0.08$ .

As is predicted by theory[2] and presented in fig.5, SNR maintains at a similar level when  $\alpha$  grows larger in the joint weak measurement scheme, because the measurement error increases along with the signal. Consider the fact that SNR grows along with the increasing signal in the weak value amplification scheme[22], it implies that the SNR of using weak value amplification will be higher than that of joint weak measurement when  $\tau$  grows large enough. In that case, imaginary weak value should involve and the harm of the QWP must be conquered, by e.g. applying broadband wave plate, but it is beyond the scope of our current work.

#### IV. CONCLUSION

Based on the idea of joint weak measurement utilizing maximum-likelihood estimation method, we generalized a formalism of weak measurement scheme with arbitrary post-selection for the purpose of parameter estimation. Especially, we applied this theory to the time-delay measurement task and discuss the *balanced*- and *unbalanced*-postselection regimes separately. In the balanced-postselection regime, we derived a formula estimating the time-delay only depends on the collected data. On the other hand, in the unbalanced-postselection regime, we found that our formula can be approximated to the well known weak-value amplification formula.

Our theory is then well testified by a time-delay measure experiment. From the experiment results, we compare the performances of weak-value amplification scheme and joint weak measurement scheme. Under the similar experimental conditions, the signal-to-noise ratio of using joint weak measurement scheme remains higher than 12 dB when the time delay to be measured approaches the ultimate precision limit of the weak-value amplification scheme. Furthermore, the balanced-postselection regime combined with joint weak measurement is robust against not only the misalignment errors but also the wavelength-dependence of the optical components, which appears to be a good approach for achieving higher measurement precision with convenient laboratory equipments.

#### Acknowledgments

This work was supported by the National Natural Science Foundation of China (Grants No. 61170228No. 61332019 61471239), and the Hi-Tech Research and Development Program of China (Grant No: 2013AA122901).

#### Appendix A: Phase retardation of compound binary zero-order wave-plate

When light propagate through a uniaxial crystal plate, the phase delay between the ordinary light and extraordinary light is,

$$\delta = \frac{2\pi}{\lambda} (n_e - n_o) L \sin^2 \eta, \quad (A1)$$

where  $\lambda$  is the wavelength,  $n_o$  and  $n_e$  stand for refractive index of ordinary and extraordinary light, respectively.  $L = \frac{h}{\cos \eta_i}$  means the path length propagating in the crystal.  $\eta$  is the angle between the normal line and the OA,  $\eta_i$  is the angle between the light velocity in the crystal and the normal line. And  $h$  is the thickness of the plate. For simplicity, we establish a Cartesian coordinates showed in Fig.6 to calculate  $C = L \sin^2 \eta$  in the crystal which we call the effective path length in the next. The origin is coincident with the point of incidence. X-Z plane is on the surface of the plate. And the OA is paralleled with Z-axis. It's obvious that  $L^2 = x^2 + y^2 + z^2$ ,  $L^2 \sin^2 \eta =$

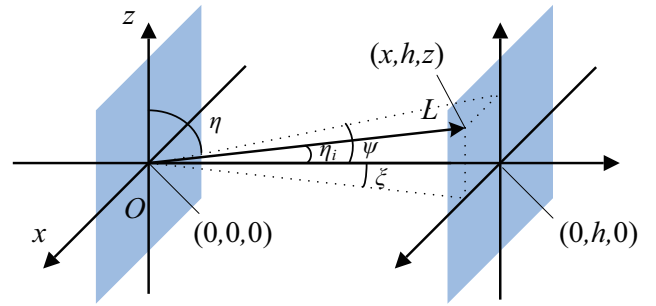


FIG. 6: (Color online). Coordinate system of single birefringent waveplate.

$x^2 + y^2$ , and

$$C = L \sin^2 \eta = \frac{x^2 + y^2}{\sqrt{x^2 + y^2 + z^2}}. \quad (A2)$$

The exit point is  $(x, h, z)$ . And the effective path length could be obtain by replacing  $h$  by  $y$ . In our experiment, the pivot is around the OA, we define the azimuth angle and elevation angle as  $\xi$  and  $\psi$  respectively, so

$$\begin{aligned} x^2 + h^2 &= h^2 / \cos^2 \xi, \\ z^2 + h^2 &= h^2 / \cos^2 \psi, \end{aligned} \quad (A3a)$$

and we could deduce that

$$x^2 + y^2 + z^2 = \frac{h^2 (1 - \sin^2 \xi \sin^2 \psi)}{\cos^2 \xi \cos^2 2\psi}, \quad (A3b)$$

inserting Eq.A2 and Eq.A3 into Eq.A1, we could get the general expression of the phase retardance of oblique incidence on a crystal plate

$$\delta = \frac{2\pi}{\lambda} (n_e - n_o) C = \frac{2\pi (n_e - n_o) h \cos \psi}{\sqrt{\cos \xi (1 - \sin^2 \xi \sin^2 \psi)}}. \quad (A4)$$

The compound binary plate is built by combining two multi-order wave plates to obtain an zero-order phase delay by aligning the fast axis of one plate with the slow axis of the other. The retardance could be expressed as

$$\delta = \frac{2\pi}{\lambda} (n_e - n_o) (h_1 - h_2). \quad (A5)$$

Fig.7 represent the Cartesian coordinates when light go through the second plate while the Fig.6 still shows the incidence on the first plate. The origin overlaps with the exit point of the first plate. Since the OA of the second plate is perpendicular to the first one's, the coordinate system is rotating by 90°. Let the subscripts denote the two plates. We neglect the refringence between the two plates, and suppose that  $\xi$  in Fig.7 is approximately equal to  $\psi$  in Fig.6, we can derive that

$$\begin{aligned} z_1/h_1 &= x_2/h_2, \\ x_1/h_1 &= -z_2/h_2. \end{aligned} \quad (A6)$$

The phase delay of the compound plate is

$$\delta = \frac{2\pi}{\lambda} (n_e - n_o) (C_1 - C_2), \quad (A7)$$

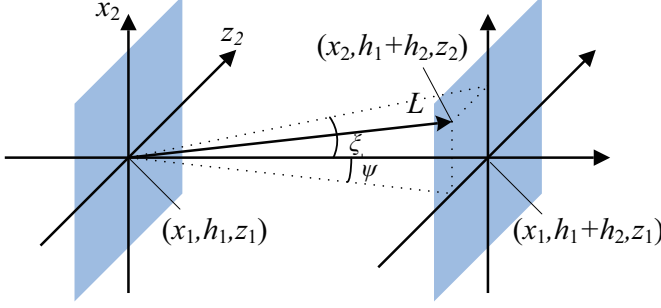


FIG. 7: (Color online). Coordinate system of the second plate in a compound wave plate.

where

$$\begin{aligned} C1 &= \frac{x_1^2 + h_1^2}{\sqrt{x_1^2 + h_1^2 + z_1^2}}, \\ C2 &= \frac{h_2(x_1^2 + h_1^2)}{h_1 \sqrt{x_1^2 + h_1^2 + z_1^2}}, \end{aligned} \quad (\text{A8})$$

combining with Eq.A2 and taking account of the relationship of those angles, we found the general expression of the phase retardance of the compound plate:

$$\delta = \frac{2\pi(n_e - n_o)(h_1 \cos \psi / \cos \xi - h_2 \cos \xi / \cos \psi)}{\lambda \sqrt{1 - \sin^2 \xi \sin^2 \psi}}. \quad (\text{A9})$$

when  $\psi = 0$  and  $\xi$  is small, Eq.A9 becomes

$$\begin{aligned} \delta &= \frac{2\pi(n_e - n_o)}{\lambda} (h_1 / \cos \xi - h_2 \cos \xi) \\ &\approx \frac{2\pi(n_e - n_o)}{\lambda} [(h_1 - h_2) + \xi^2(h_1 + h_2)/2], \end{aligned} \quad (\text{A10a})$$

and when  $\xi = 0$  and  $\psi$  is small, Eq.A9 approximates to

$$\begin{aligned} \delta &= \frac{2\pi(n_e - n_o)}{\lambda} (h_1 \cos \psi - h_2 / \cos \psi) \\ &\approx \frac{2\pi(n_e - n_o)}{\lambda} [(h_1 - h_2) - \psi^2(h_1 + h_2)/2]. \end{aligned} \quad (\text{A10b})$$

In Eq.A10, the 1st term is the plate's retardance of vertical incidence, the 2nd term means the phase delay of oblique incidence. Considering the relationship between the incidence angle  $\theta$ ,  $\psi$  and  $\xi$ , we could rewrite the 2nd term as

$$\Delta\delta = \frac{\pm\pi(n_e - n_o)(h_1 + h_2)\theta^2}{\lambda n^2} \quad (\text{A11})$$

when  $\psi = 0$  it has the positive value and the negative value could be obtain while  $\xi = 0$ . In the range of our LED spectrum,  $n_e - n_o$  is almost constant, in other words, the optical length in the crystal is unsensitive to the variation of wavelength. With the cancelling effect of the two waveplates in our experiment, the time delay induced by the pivot is

$$\tau = \frac{\Delta\delta \lambda}{2\pi c} = \frac{\pm(n_e - n_o)(h_1 + h_2)\theta^2}{2c\lambda n^2} \quad (\text{A12})$$

where  $c$  is the the speed of light in vacuum.

## Appendix B: Effect of wavelength-dependent quarter-wave plate

The postselection in our experiment consists of a quarter-wave plate and a linear polarization beam splitter(PBS). For using ideal quarter-wave plate Eq.(11) is established, however in practice optical components are wavelength-dependent. A quarter-wave plate with its optical axis at 45° direction and central angular frequency of  $\omega_0$  can be described by a Jones matrix as:

$$\begin{aligned} U_{\lambda/4} &= \frac{1}{2} \begin{pmatrix} 1 & -1 \\ 1 & 1 \end{pmatrix} \begin{pmatrix} e^{-i\omega\tau_0} & 0 \\ 0 & e^{i\omega\tau_0} \end{pmatrix} \begin{pmatrix} 1 & 1 \\ -1 & 1 \end{pmatrix} \\ &= \begin{pmatrix} \cos \omega\tau_0 & -i \sin \omega\tau_0 \\ -i \sin \omega\tau_0 & \cos \omega\tau_0 \end{pmatrix} \end{aligned} \quad (\text{B1})$$

where  $\tau_0 = \frac{\pi}{4}/\omega_0$ , and  $\omega$  is the angular frequency of the light.

Denote the linear polarization state selected by PBS is  $|\varphi_f\rangle$ , the postselection of  $|\varphi'_f\rangle$  can be divided as

$$\begin{aligned} \langle \varphi'_f | \hat{U}_{int} | \varphi_i \rangle | \phi \rangle \\ = (\langle \varphi_f | \hat{U}_{\lambda/4} ) \hat{U}_{int} | \varphi_i \rangle | \phi \rangle. \end{aligned} \quad (\text{B2})$$

Obviously,  $|\varphi'_f\rangle = \hat{U}_{\lambda/4}^\dagger |\varphi_f\rangle$  is frequency-dependent. Combining with Eq.(B1) and the expressions of  $|\varphi_{f1}\rangle = \cos \gamma |H\rangle + \sin \gamma |V\rangle$  and  $|\varphi_{f2}\rangle = \sin \gamma |H\rangle - \cos \gamma |V\rangle$ , we can derive  $|\varphi'_{f1}\rangle = (\cos \omega\tau_0 \cos \gamma + i \sin \omega\tau_0 \sin \gamma) |H\rangle + (\cos \omega\tau_0 \sin \gamma + i \sin \omega\tau_0 \cos \gamma) |V\rangle$  and  $|\varphi'_{f2}\rangle = (\cos \omega\tau_0 \sin \gamma - i \sin \omega\tau_0 \cos \gamma) |H\rangle + (-\cos \omega\tau_0 \cos \gamma + i \sin \omega\tau_0 \sin \gamma) |V\rangle$ . Consequently, the weak values can be calculated as

$$\begin{aligned} A_{w1} &= \frac{\langle \varphi'_{f1} | \hat{A} | \varphi_i \rangle}{\langle \varphi_{f1} | \varphi_i \rangle} \\ &= \frac{(\cos \omega\tau_0 + i \sin \omega\tau_0)(\cos \gamma - \sin \gamma)}{(\cos \omega\tau_0 - i \sin \omega\tau_0)(\cos \gamma + \sin \gamma)} \\ &= e^{i2\omega\tau_0} \frac{\cos \gamma - \sin \gamma}{\cos \gamma + \sin \gamma} \\ A_{w2} &= \frac{\langle \varphi'_{f2} | \hat{A} | \varphi_i \rangle}{\langle \varphi_{f2} | \varphi_i \rangle} \\ &= \frac{(\cos \omega\tau_0 + i \sin \omega\tau_0)(\cos \gamma + \sin \gamma)}{(\cos \omega\tau_0 - i \sin \omega\tau_0)(\sin \gamma - \cos \gamma)} \\ &= e^{i2\omega\tau_0} \frac{\cos \gamma + \sin \gamma}{\sin \gamma - \cos \gamma} \end{aligned} \quad (\text{B3})$$

In this case,  $A_{wj}$  can not be taken outside of the integral of Eq.(7). Compare the results shown in fig.3 and fig.4 we can see that in the balanced postselection regime, Eq.(9) provides a good approximation, while in the unbalanced postselection regime the wavelength-dependency of the quarter-wave plate involves an unneigligible deviation.

- [3] O. Hosten and P. Kwiat, *Science* **319**, 787 (2008).
- [4] D. Starling, et al., *Phys. Rev. A* **80**, 041803 (2009).
- [5] G. Viza, et al., Weak-values technique for velocity measurements, *Opt. Lett.* **38**, 2949 (2013).
- [6] J. Dressel, M. Malik, F. Miatto, A. Jordan, and R. Boyd, Colloquium: Understanding Quantum Weak Values: Basics and Applications, *Rev. Mod. Phys.* **86**, 307 (2014).
- [7] G. Strübi, PhD thesis, 2013.
- [8] A. Jordan, J. Martínez-Rincón and J. C. Howell, Technical Advantages for Weak-value Amplification: When Less is More, *Phys. Rev. X* **4**, 011031 (2014).
- [9] G. Viza, et al., Experimentally quantifying the advantages of weak-values-based metrology, *arXiv:1410.8461v1* (2014).
- [10] N. Brunner and C. Simon, *Phys. Rev. Lett.* **105**, 010405 (2010).
- [11] C. Li, X. Xu, J. Tang, J. Xu and G. Guo, *Phys. Rev. A* **83**, 044102 (2011).
- [12] X. Xu, et al., Phase Estimation with Weak Measurement Using a White Light Source, *PRL* **111**, 033604 (2013).
- [13] G. Knee and E. Gauger, When Amplification with Weak Values Fails to Suppress Technical Noise, *Phys. Rev. X* **4**, 011032 (2014).
- [14] L. Zhang, A. Datta, and A. Walmsley, Precision metrology using weak measurements, *arXiv:1310.5302v1* (2013).
- [15] A. Jordan, et al., Heisenberg scaling with weak measurement: A quantum state discrimination point of view, *arXiv:1409.3488v1* (2014).
- [16] Y. Aharonov, D. Albert and L. Vaidman, *Phys. Rev. Lett.* **60**, 1351 (1988).
- [17] R. Jozsa, Complex weak values in quantum measurement, *Phys. Rev. A* **76**, 044103 (2007).
- [18] T. Koike and S. Tanaka, *Phys. Rev. A* **84**, 062106 (2011).
- [19] S. Pang, and T. Brun, Improving the precision of weak measurements by postselection, *arXiv:1409.2567v1* (2014).
- [20] G. Bié Alves, et al., Weak-value amplification as an optimal metrological protocol, *arXiv:1410.7415v1* (2014).
- [21] C. Ferrie and J. Combes, Weak Value Amplification is Suboptimal for Estimation and Detection, *Phys. Rev. Lett.* **112**, 040406 (2014).
- [22] D. Starling, et al., *Phys. Rev. A* **82**, 011802(R) (2010).
- [23] C. Helstrom, *Quantum detection and estimation theory*, Academic press (1976).
- [24] M. Nielsen and I. Chuang, *Quantum computation and quantum information*, Cambridge University Press, 2000.
- [25] H. Bachor and T. C. Ralph, *A Guide to Experiments in Quantum Optics* (2nd Edition), WILEY-VCH (2004).
- [26] Hua Li, Song Lianke, and Li Guohua. "Orientation effect on phase retardation of compound binary zero-order waveplate." *Acta Optica Sinica* **22.12** (2002): 1438-1443.